Optical pumping of Rb vapor using high-power $Ga_{1-x}Al_xAs$ diode laser arrays

W.J. Cummings,[1] O. Häusser,[1,2] and W. Lorenzon[2]
[1] *TRIUMF, 4004 Wesbrook Mall, Vancouver, British Columbia, Canada V6T 2A3*
[2] *Simon Fraser University, Burnaby, British Columbia, Canada V5A 1S6*

D. R. Swenson
Los Alamos National Laboratory, MS H838, Los Alamos New Mexico 87545

B. Larson
Department of Physics and Astronomy, Ohio University, Athens, Ohio 45701-2979
(Received 25 October 1994)

The use of high-power $Ga_{1-x}Al_xAs$ diode laser arrays for optical pumping of Rb vapor has been examined both theoretically and experimentally. Our studies show that large atomic polarizations can be obtained using the broad spectral output of a diode laser array if the Rb resonance line is collisionally broadened by several atmospheres of a buffer gas. The objective was to study the effectiveness of diode laser arrays as light sources for optically pumped spin-exchange polarized ^{3}He targets. The average Rb polarization was deduced at three different Rb vapor pressures using the polarization induced in the ^{3}He buffer gas. The largest ^{3}He polarization observed was 53% using a 20-W diode array with 1.9-nm full width at half maximum spectral width in 10.5 amagat of ^{3}He. This result compares favorably with other light sources for this target. The measured average Rb polarizations are compared to theoretical calculations.

PACS number(s): 32.80.Bx, 42.55.Px, 42.62.−b, 29.25.Pj

I. INTRODUCTION

In the past several years, the development of high-pressure, highly polarized ^{3}He samples has facilitated many important experiments in atomic, nuclear, and particle physics. In these high-pressure targets, ^{3}He atoms are polarized by spin-exchange collisions with optically pumped Rb metal vapor. ^{3}He targets polarized in this manner have been used for a variety of experiments utilizing muon, pion, neutron, polarized proton, and polarized electron beams [1–10]. The experiments included deep inelastic scattering of polarized electrons from polarized ^{3}He [1] to measure the spin structure function of the neutron, polarization of epithermal neutron beams using polarized ^{3}He as a spin filter [2–4], polarized proton scattering from polarized ^{3}He [5,6], production of polarized muonic ^{3}He [7,8], and elastic pion scattering from polarized ^{3}He [9,10].

The work presented in this paper was performed using the spin-exchange polarized ^{3}He target developed at TRIUMF [11]. This target was used for the proton and pion scattering experiments mentioned above. In a spin-exchange polarized ^{3}He target, the polarization of the ^{3}He nucleus occurs during collisions with spin polarized Rb atoms via the contact hyperfine interaction between the ^{3}He nuclear spin and the Rb atomic spin. The Rb atoms are spin polarized by optical pumping of the $5\,^2S_{1/2} \rightarrow 5\,^2P_{1/2}$ transition ($D1$ spectral line) using circularly polarized light propagating parallel to a weak magnetic field. Since the time scale for spin-exchange [10 h for a Rb density of $(3-4)\times 10^{14}$ cm^{-3}] is much larger than the optical pumping time scale (1 ms), the steady state ^{3}He polarization is directly proportional to the average Rb polarization. The proportionality between the ^{3}He polarization and the Rb polarization will be used to estimate values for the average Rb polarization.

The optical pumping of Rb for ^{3}He polarization was first accomplished using resonance lamps, then dye lasers, and more recently Ti:sapphire lasers. The use of a diode array as the optical pumping source for the production of polarized ^{3}He by spin-exchange with Rb vapor was demonstrated first by Chupp and Wagshul [12]. It was shown that the 0.5-W diode array could produce polarizations comparable to dye lasers, in spite of its much wider linewidth. Shortly after publication of their work, the Ti:sapphire laser was introduced [11] with cw outputs approaching 6 W, making it the best choice for this application. Ti:sapphire lasers were adopted for most of the recently performed experiments described above. The power available from diode arrays has increased significantly over the past few years. The prospect that a currently available high-power (20-W) diode array could match the optical pumping efficiency of a Ti:sapphire laser at an order of magnitude less cost has motivated us to reexamine theoretically and experimentally the use of diode arrays.

II. THEORY

The theory of optical pumping of Rb vapor in the presence of a He buffer gas has been presented many times in the literature [11–15]. As mentioned above, Ref. [12] previously examined the case of a broadband $Ga_{1-x}Al_xAs$

diode laser light source. Therefore, only formulas relevant to the present calculations are presented here. The most important formulas for these studies have been derived from the solution to the optical pumping rate equation under the following assumptions. It has been assumed that collisional mixing in the excited $5\,^2P_{1/2}$ state due to a small amount of N_2 quench gas results in equal probability of deexcitation to the $m_s = +1/2$ and $m_s = -1/2$ substates of the ground state. In addition, fluorescence of excited state Rb atoms has been ignored. The polarization of the Rb vapor as a function of distance in a uniform ^{3}He buffer gas is

$$P_{\rm Rb}(z) = \frac{\gamma^+(z)}{\gamma^+(z) + \Gamma_{\rm SD}} \tag{1}$$

and the power absorbed inducing that polarization is

$$\Delta I^+(z) = -\frac{\Delta z[\rm Rb]\gamma^+(z)\Gamma_{\rm SD}}{\gamma^+(z) + \Gamma_{\rm SD}}. \tag{2}$$

In these expressions, I^+ is the number of circularly polarized photons cm^{-2} s^{-1}, [Rb] is the Rb density in atoms cm^{-3}, Δz is the distance step in cm, $\Gamma_{\rm SD}$ is the spin-destruction rate in s^{-1}, and $\gamma^+(z)$ is the photon absorption rate for circularly polarized photons. This rate is defined as

$$\gamma^+(z) = \int \Phi^+(\nu, z)\sigma(\nu)d\nu, \tag{3}$$

where $\Phi^+(\nu, z)$ is the flux of circularly polarized photons (GHz^{-1} cm^{-2} s^{-1}) at a frequency ν and $\sigma(\nu)$ is the cross section for absorption of linearly polarized photons by unpolarized Rb vapor near the Rb $D1$ line. This resonant cross section is centered around the wavelength λ_0 (frequency ν_0) and can be described as [11]

$$\sigma(\delta\nu) = \frac{\lambda_0^2}{8\pi}\Gamma_{\rm nat}\left[\frac{\Gamma}{(\delta\nu)^2 + (\Gamma/2)^2} + \frac{b\delta\nu}{\Gamma}e^{-|\delta\nu|/\Gamma_a}\right], \tag{4}$$

where $\delta\nu = (\nu - \nu_0)$ is the detuning parameter in GHz, Γ is the collisionally broadened width, and $\Gamma_{\rm nat}$ is the natural linewidth (5.66 MHz). The remaining parameters describe the asymmetric portion of the cross section and have a negligible effect on the results presented here.

Rb spin-destruction is dominated by Rb-Rb and Rb-He binary collisions. The total Rb spin-destruction rate $\Gamma_{\rm SD}$ can be expressed as the sum of these contributions,

$$\Gamma_{\rm SD} = \gamma_{\rm Rb} + \gamma_{\rm SE} + \gamma_{\rm SR}. \tag{5}$$

The first term $\gamma_{\rm Rb}$ describes the contribution from Rb-Rb collisions

$$\gamma_{\rm Rb} = \langle\sigma_{\rm SD}v\rangle[\rm Rb]. \tag{6}$$

This rate has been measured [11,16] and we use the result of Ref. [11]: $\langle\sigma_{\rm SD}v\rangle = 8.3 \times 10^{-13}$ cm^3 s^{-1}. The other terms ($\gamma_{\rm SE}$ and $\gamma_{\rm SR}$) represent the spin-destruction rate from the He-Rb spin-exchange and spin-randomization collisions, respectively. Of these rates, which are both proportional to [^{3}He], the ^{3}He density in amagats (an amagat is a unit of density corresponding to 1 atm at 0 °C), the nuclear spin independent $\gamma_{\rm SR}$ has been measured [17] to be an order of magnitude larger than $\gamma_{\rm SE}$. These earlier measurements of Rb spin destruction in the helium isotopes [17] were made for He densities less than 0.7 amagat at a temperature of 578 K and cannot be directly applied to the present work. Larson *et al.* [11] have measured $\Gamma_{\rm SD}$ as a function of He density near 450 K. Using their results, we calculate the total contribution to the spin-destruction rate from Rb-^{3}He collisions. For the 10.5-amagat cell used here, we obtain $\gamma_{\rm SE} + \gamma_{\rm SR} = 610$ s^{-1}. By comparison, for [Rb]$= 4.0 \times 10^{14}$ cm^{-3}, $\gamma_{\rm Rb}$ contributes only 332 s^{-1}. In previous work [2,3,12–14], the contributions to $\Gamma_{\rm SD}$ from Rb-He collisions were not included. In this discussion, we have ignored a small contribution to $\Gamma_{\rm SD}$ from N_2-Rb collisions. This contribution, which is due to the 0.13 amagat N_2 quench gas in the cell, can be estimated from previous measurements [17] performed at similar N_2 densities. From these earlier measurements, the size of this contribution is limited to < 32 s^{-1}.

The salient features of diode laser arrays for the optical pumping of Rb are illustrated in Fig. 1. The Rb $D1$ absorption cross section is shown as the solid curve. The asymmetric part of the cross section has been ignored and the width has been set to 235 GHz, the measured width for the 10.5-amagat cell used in this work. Also shown as the dotted curve is a 1.9-nm full width at half maximum (FWHM) Gaussian spectral profile of a diode laser array. This line shape and width are similar to the diode laser used for the measurements in this paper. Even for the high-density ^{3}He cell, the linewidth of the array is much wider than the absorption linewidth. This makes the

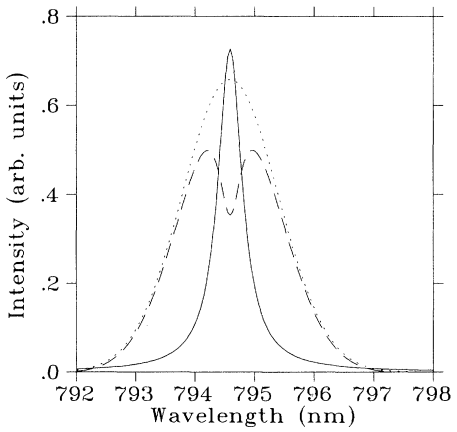

FIG. 1. Absorption of diode laser light used for optical pumping. The solid curve shows the line shape of the Rb $D1$ absorption cross section, which has been collisionally broadened from the presence of 10.5 amagat of ^{3}He. The dotted curve shows the Gaussian line shape of a 1.9-nm FWHM diode laser array. This linewidth is much larger than the absorption cross section. The dashed curve shows the diode laser line shape after it has passed through 1 cm of Rb vapor ([Rb]$= 4.0 \times 10^{14}$ cm^{-3}). Even though much of the power at the central frequencies of the diode laser has been absorbed, the diode laser continues to optically pump the Rb.

optical pumping efficiency relatively insensitive to laser detuning effects. The dotted curve in Fig. 1 shows the diode array line shape after the circularly polarized light has passed through 1.0 cm of Rb vapor at a density of 4.0×10^{14} cm^{-3}. Most of the power at the wavelengths near the absorption maximum has been spent. However, the remaining power can still be absorbed and continue optical pumping. Thus the large bandwidth of the diode laser array can be effectively used to pump the Rb vapor.

As in the previous work by Chupp and Wagshul [12], we have calculated the Rb polarization [Eq. (1)] by numerically evaluating the γ^+ integral [Eq. (3)] and then removing the appropriate power density [Eq. (2)] from the incident laser light. The incident laser light was assumed to be 100% circularly polarized and the frequency profile was assumed to be Gaussian.

Figure 2 shows the result of using a Gaussian approximation for the laser spectral line shape: the Rb polarization as a function of distance in 7 amagat of uniform ^{3}He gas with Rb vapor density of 4.0×10^{14} cm^{-3}. The solid line shows the polarization induced from 15 W of light from a diode laser array having a spectral linewidth of 1.9 nm FWHM and a Gaussian profile. This should be compared with the dotted line in Fig. 2, which shows the calculation of the polarization induced by the diode laser actually used. The calculation was modified to include the measured diode line shape and power (see below). Since the results are similar, and to preserve generality, the Gaussian line shape was used for the remainder of the theoretical calculations.

Figure 3 shows the Rb polarization vs distance for four different ^{3}He densities between 3 amagat and 10.5 amagat. In each case the solid line represents the polarization induced by 15 W of light from a diode laser array having a spectral linewidth of 1.9 nm FWHM. For comparison,

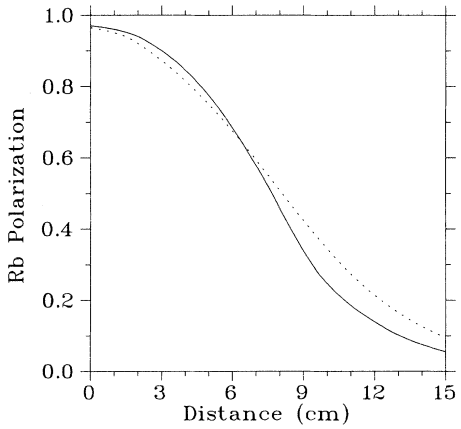

FIG. 2. Comparison of a 15-W Gaussian 1.9-nm FWHM diode laser array with the diode laser actually used. The Rb polarization vs distance is shown for a diode laser propagating through 7.0 amagat of ^{3}He gas with [Rb]= 4.0×10^{14} cm^{-3}. The solid line was calculated for a 15-W diode laser array with a Gaussian line shape (1.9 nm FWHM). This is to be compared with the dotted line, which was calculated using the measured power and line shape from the diode laser used in this paper.

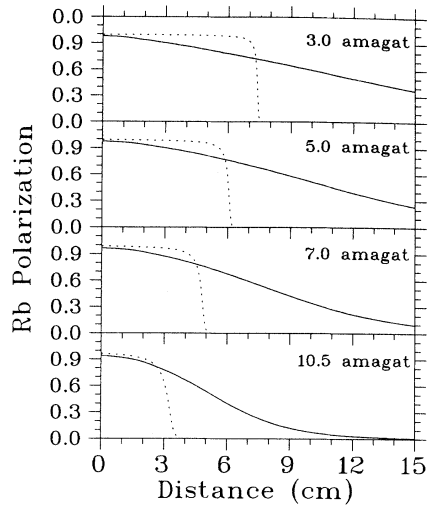

FIG. 3. Rb polarization vs ^{3}He density. Shown is the calculated Rb polarization vs distance for four different densities of the ^{3}He buffer gas. In each plot, the solid line is the result for a 15-W diode laser array with a Gaussian line shape (1.9 nm FWHM). By comparison, the dotted line in each plot shows the results of the calculation with an 8-W Ti:sapphire light source as input.

we show as the dotted lines in Fig. 3 the polarizations induced from 8 W of Ti:sapphire laser light (FWHM of 0.04 nm), which is typically available from two Ar^+ pumped laser systems. All calculations assume that the full rated power of the laser beam can be uniformly expanded to the nominal 6.5×4.5 cm^2 cross sectional size of the ^{3}He glass cell used in the LAMPF experiment [10] for which these calculations were originally done. For densities above a few amagats, the diode laser array compares favorably with Ti:sapphire lasers as a light source for optical pumping of Rb.

Our calculations show that a high-power diode laser array can provide the high Rb polarizations necessary for effectively polarizing ^{3}He by spin-exchange. To experimentally test these predictions, we have measured the ^{3}He polarization induced by optically pumping one of the TRIUMF targets using only a diode laser array.

III. EXPERIMENTAL TECHNIQUE

The targets used in our experiments are Corning 1720 glass cells filled with several atmospheres of ^{3}He gas and with smaller amounts of N_2 to allow radiationless deexcitation of the Rb resonance lines. A small amount of Rb metal is deposited in the cell, which is partially vaporized when the cell is heated. The glass cell is mounted in an oven made of the polyimide VESPEL. Windows consisting of two layers of 25-μm kapton separated by an air gap of 6.4 mm were used to reduce heat loss and thermal gradients within the oven. The oven was operated at a temperature of 450 K to produce a Rb density of 4×10^{14} cm^{-3}. A vertical holding field of 3 mT is produced by a set of 1-m diam Helmholtz coils. The techniques used

in the manufacture and operation of the cells have been published elsewhere [11,19].

For the measurements presented in this paper, we used a cell that was previously used at TRIUMF as a polarized ^{3}He target for elastic pion scattering measurements [24]. This cigar shaped cell is 8 cm long, has a 2.4 cm inner diameter, and an inner gas volume of about 35 cm^3. The glass wall thickness in most of the cell is 1 mm, but is considerably thinner (100 μm) in the end caps where the beam enters and exits the target. The cell contains 10.5 amagat of ^{3}He and about 0.13 amagat of N_2. This ^{3}He cell is one of the highest density cells made at TRIUMF. It was chosen for this work to take full advantage of the collisionally broadened width of the $D1$ line.

The equipment required for operating the diode laser was modest. Figure 4 is a diagram of the setup, which consisted of the laser, a water cooled heatsink, a water chiller, a dc power supply, circuitry and interlocks for protecting the laser, and optics for collimating the beam. The laser (Spectra Diode Laboratories model SDL-3460-S) is a 1 cm long by 1 μm wide linear array of 24 $Ga_{1-x}Al_xAs$ diodes, which produces 20-W cw output with 30 A of drive current. The laser cooling was provided by a water and ethylene glycol chiller (Neslab, HX-75 modified) capable of 14 liter/min flow at 2.7 bar with temperature control (accuracy $\pm$ 0.5 °C). The laser was mounted to a heat sink (SDL-830-S) using a 50.0-μm-thick layer of indium foil to increase the thermal contact. The temperature of the diode case was monitored by thermistors attached to the mounting screws. Tuning the frequency of the laser was accomplished by changing the temperature settings of the chiller. Figure 5 shows measurements of the laser frequency distribution carried out with a 0.5-m monochromator (100 μm slit width) for two different chiller settings. Operation at the $D1$ resonance line of Rb at 794.8 nm required a case temperature of -1.0 °C. Because of the low operating temperature, the insulating housing was continuously purged with dry nitrogen from the boiloff of a liquid nitrogen Dewar to prevent condensation, which could damage the laser facet. A less expensive chiller could be used if shorter wavelength diodes are purchased. A more efficient heat sink would also lessen the demands on the chiller. Operation at a temperature above the dew point would not require the dry nitrogen purge.

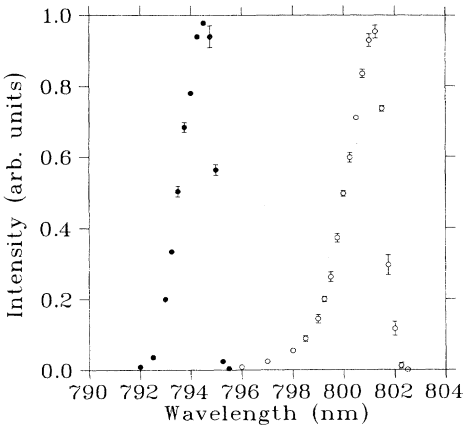

FIG. 5. Measurements of the diode laser line shape at two different temperatures. The open circles represent the measurements at a case temperature of T = 26 °C (chiller, T = 18 °C) and give a centroid of 800.6 nm. The filled circles give the same data at a case temperature of T = -2.7 °C (chiller: T = -10 °C) and have a centroid of 794.2 nm. The error bars shown were calculated by doing two consecutive scans and comparing the results. For the points where the error bars cannot be seen, the error is less than the size of the plotting symbol. Interesting features of these data are the asymmetric frequency distribution with a 1.9 nm FWHM, which narrowed by 10% at the lower temperature, and the frequency distribution, which appears smooth, without mode structure. The lack of mode structure is a result of the large number of independent emitters.

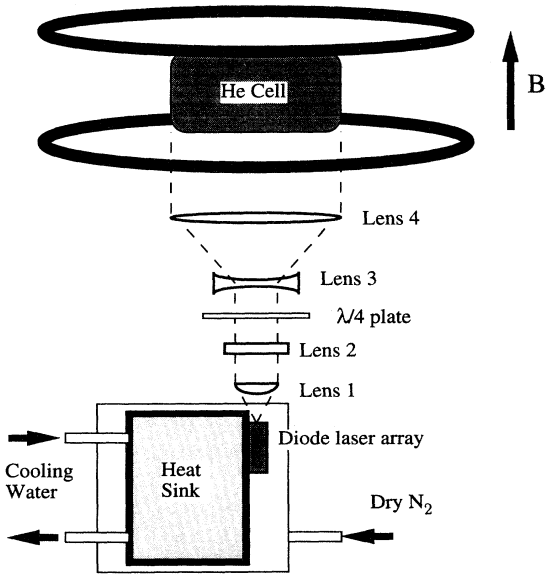

FIG. 4. Schematic diagram of the optical pumping apparatus.

The laser diode is powered by a dc power supply capable of delivering up to 30 A at 3 V. Two additions were made to circuitry recommended by the manufacturer to give added protection. A primary consideration is protecting the diode from current transients that raise the optical power above the damage threshold of the facet. Our first laser was progressively damaged by 60-A 1-μs current spikes that were induced by closing a shorting switch at high current (the manufacturer recommends a switch for short circuiting the diode. The diode is shorted out of the circuit before turning the power supply on or off or before making adjustments). To prevent a recurrence, a string of silicon power diodes across the laser was added to clamp the voltage to a safe level (within a few tenths of a volt of the voltage drop across the diode). The turnoff procedure was also changed: the current was first reduced to zero and then the shorting switch was closed before turning off the power supply. The other addition to the circuitry was a flow meter with an interlock to turn the power supply off if the cooling water flow

to the laser was interrupted. It was found that turning the supply off was less likely to cause current transients than the original scheme of closing the shorting switch.

The light output of the diode array is highly divergent and asymmetric, with a nonuniform power distribution. The manufacturer specifies the beam divergence angle FWHM as 30° perpendicular to the diode strip and 10° parallel to the strip. The intensity is greater at the edges of the beam than the center. An additional nonuniformity arises because the 24 beamlets do not fully overlap. The beam is collimated and expanded using four lenses as shown in Fig. 4. The first lens was cylindrical with a focal length of 12.7 mm. It is spaced one focal length from the diode to minimize the divergence perpendicular to the diode strip. The second lens is cylindrical with a focal length of 40 mm. It is spaced approximately one focal length from the diode array to minimize the divergence parallel to the diode strip. The two lenses produce a collimated beam, which passes through the quarter wave plate. It is important that the light is linearly polarized and parallel at the quarter wave plate, to minimize elliptical polarization. The detrimental effect of elliptical polarization is discussed below. The linear polarization was measured using a Glan polarizer and the extinction ratio was 20:1. After the quarter wave plate, a Gallilean beam expander expands the beam size to the size of the glass cell.

IV. DATA ANALYSIS

The effectiveness of the diode laser array for optical pumping of Rb vapor was measured indirectly by monitoring the ^{3}He polarization in the glass cell. The polarization of the ^{3}He gas was measured using adiabatic fast passage (AFP) nuclear magnetic resonance (NMR). This signal was normalized by comparing to the much smaller AFP NMR signal from a water filled glass cell of similar size. A detailed description of this technique for measuring the polarization can be found elsewhere [3,11,13,14,18].

For the present measurements, the ^{3}He polarization as a function of time is shown in Fig. 6. The polarization was measured approximately every 8 h over a period of about 80 h. These ten measurements are shown as the filled circles on Fig. 6. It is well known [11,13] that the time evolution of the ^{3}He polarization should follow the curve

$$P(t) = M + (P_i - M)e^{-(\gamma_{SE}+\Gamma)t}, \tag{7}$$

where P_i is the initial ($t = 0$) and M is the asymptotic ($t \to \infty$) value of polarization, which is given by

$$M = \frac{\gamma_{SE} P_{Rb}}{\gamma_{SE} + \Gamma}, \tag{8}$$

where γ_{SE} is the spin-exchange rate and Γ is the total spin-relaxation rate from effects other than spin-exchange. The spin-exchange rate is given by

$$\gamma_{SE} = \langle \sigma_{SE} v \rangle [\mathrm{Rb}], \tag{9}$$

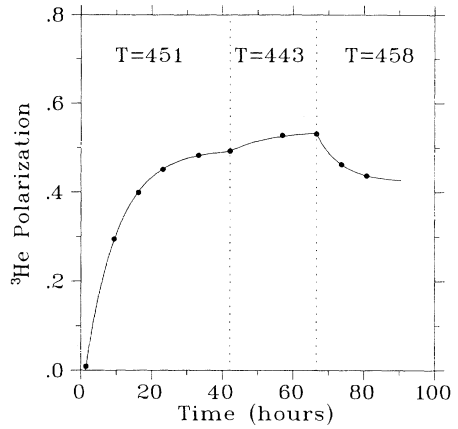

FIG. 6. Measured ^{3}He polarization is shown as a function of time. The closed circles show the measurements of the ^{3}He polarization by AFP NMR. The solid line is a fit to the data (see the text). The maximum polarization was 53%.

where $\langle \sigma_{SE} v \rangle$ is the velocity averaged spin-exchange cross section. The temperature of the glass cell determines the Rb number density.

In previous work [11], the value of Γ was measured through the decay of the ^{3}He polarization at room temperature (where the Rb vapor pressure is so low that there is no spin-exchange contribution) and it was assumed to be independent of temperature. This cold spin-relaxation rate has been measured for the cell used for these data and has the value $\Gamma(300) = 1/59\ \mathrm{h}^{-1}$. However, a recent publication [19] has shown that this is not a valid assumption. They calculate the spin relaxation in ^{3}He due to the magnetic dipole-dipole coupling between the ^{3}He nuclear spins and find that this relaxation rate can be expressed as (at 23 °C)

$$\Gamma_{\mathrm{dipole}} = \frac{[^3\mathrm{He}]}{744}\ \mathrm{h}^{-1}. \tag{10}$$

For our 10.5-amagat cell, this leads to a contribution to the cold relaxation rate of $1/70.8\ \mathrm{h}^{-1}$. This theoretical calculation [19] of the dipolar relaxation rate is consistent with empirical limits based on fitting observed relaxation rates in ^{3}He cells of various densities [20]. The difference between our measured cold relaxation rate and the prediction from the dipolar relaxation interaction is due to other spin-relaxation interactions caused by magnetic field inhomogeneities, wall collisions, and collisions with paramagnetic impurities. Therefore, the total ^{3}He spin-relaxation rate can be expressed as the sum of two contributions

$$\Gamma = \Gamma_{\mathrm{other}} + \Gamma_{\mathrm{dipole}}. \tag{11}$$

At room temperature, the spin-relaxation rate from other interactions is given by

$$\Gamma_{\mathrm{other}} = \Gamma(300) - \Gamma_{\mathrm{dipole}}, \tag{12}$$

which yields a value of $\Gamma_{\mathrm{other}} = 1/354\ \mathrm{h}^{-1}$. Newbury and collaborators [19] show that the magnetic dipolar

TABLE I. Results of a fit to the ^{3}He polarization data. Fitted parameters are shown with both fitting and systematic errors. See the text for details.

T (K)	[Rb] (10^{14})	Γ^{-1} (h)	P_i	$(\gamma_{SE})^{-1}$ (h)	M
451	3.95	65.1±2.5	0.010±0.001	10.68±0.01±0.57	0.498±0.001±0.025
443	2.75	64.9±2.5	0.492	15.2	0.539±0.002±0.027
458	5.37	65.3±2.5	0.531	7.9	0.423±0.001±0.021

spin relaxation has a temperature dependence that reduces the spin relaxation with increasing temperature. Therefore, the Γ used in Eq. (7) must be extrapolated to the temperature used. The extrapolation of the magnetic dipolar contribution Γ_{dipole} has been performed using the calculation shown in Fig. 2 of Newbury *et al.* [19]. The temperature dependence of the other relaxation interactions Γ_{other} is unknown and introduces a systematic error to our extrapolation. We have performed the extrapolation assuming that there is no temperature dependence of Γ_{other}. These results are shown in Table I for the temperatures of our measurements. The systematic error on the extrapolation has been estimated by using two very different models for the temperature dependence of Γ_{other}. If the spin-flip probability per interaction is small, the relaxation rate scales with $T^{-1/2}$. If the relaxation mechanism is rare interactions with trace impurities (assuming no temperature dependence for the impurity density) in the sample, the relaxation rate scales with collision frequency or $T^{1/2}$. The systematic error has been estimated by using these models as extrema of the temperature dependence of Γ_{other} and is also shown in Table I as the error on Γ. For the temperatures used in this work, the systematic error is only 4% due to the dominance of the magnetic dipolar contribution. The new values of Γ of about 1/65 h^{-1} from this extrapolation are significantly smaller than the room temperature measurement. The importance of this difference is evident in its effect on the parameters we extract from our data. In particular, it has the effect of increasing the extracted values of the average Rb polarization by 4–8 %.

The data shown in Fig. 6 were measured at three different temperatures to investigate the effect of varying [Rb]. Each temperature change is shown by a vertical dotted line in Fig. 6. The solid line shown in Fig. 6 is a fit to the data using Eq. (7). The results of this fit are summarized in Table I. For the data with T=451 K, the fit was not constrained and P_i, M, and γ_{SE} were all allowed to vary. However, for the other two temperatures the fit was constrained such that P_i was fixed to the value when the temperature was changed and γ_{SE} was extrapolated from the measured value at 451 K to the new temperature using the temperature dependence of the cross section [21] ($\sigma_{SE} \propto T^{-1}$) and the average thermal velocity ($v \propto T^{1/2}$). This leads to

$$\gamma_{SE}(T) = \frac{(451)^{1/2}[\mathrm{Rb}(T)]}{T^{1/2}[\mathrm{Rb}(451)]}\gamma_{SE}(451), \qquad (13)$$

where $\gamma_{SE}[451]$ was the value extracted from the first part of the fit and the [Rb] was determined from the empirical relationship of Killian [22]

$$\log_{10}[\mathrm{Rb}(T)] = 26.41 - 4132/T - \log_{10}T. \qquad (14)$$

Thus for the data at these two temperatures (443 K and 458 K) the only adjustable parameter was M. For each fitted parameter shown in Table I, the first error is the error from the fitting procedure and the second error is from systematic effects. Errors on the fitted parameters are dominated by systematic effects. The two major sources of systematic error are the uncertainty in the extrapolation of Γ and the 5% uncertainty in the normalization of the ^{3}He polarization.

The value of $(\gamma_{SE})^{-1}$ extracted from the T = 451 K ([Rb]=3.95×10^{14}) fit to the data is 10.7 ± 0.6 h. The error in this value is dominated by the systematic error from the extrapolation of Γ to 451 K. There is no contribution from the systematic error in the normalization because it does not effect the shape of the fitted curve. Our value is in agreement with previous measurements of γ_{SE} by Larson *et al.* [11] at [Rb]=4.0 × 10^{14}. However, those measurements were made assuming no temperature dependence for Γ. If we make the same assumption, our value of $(\gamma_{SE})^{-1}$ is shifted slightly to 10.9 h and is still in agreement with Ref. [11]. It should be noted that previous measurements of γ_{SE} [2,13] have given results that are a factor of 2 higher than the present measurement and the results of Ref. [11]. This discrepancy is currently being investigated. One author [23] has called for additional measurements of σ_{SE} to resolve this issue.

The fitted values of M shown in Table I also have errors dominated by systematic effects. In this instance, the error is dominated by the 5% error in the ^{3}He polarization normalization and is unaffected by the systematic error in Γ. These fitted values of M can be used to extract the average Rb polarization in the cell, P_{Rb}, using Eq. (8) for each of the three temperatures. These values, which are listed in Table II as P_{Rb} (Expt.), are quoted with an error that receives equal contributions from the systematic errors on γ_{SE} and M. These experimental values can be directly compared to theoretical predictions of the Rb polarization induced by the diode laser. From Fig. 3, one would expect Rb polarizations near 100% in a cell that is only 2.4 cm in diameter. However, these extracted average Rb polarizations are less than 75%.

TABLE II. Comparison of the measured average Rb polarization with theoretical predictions. The error on the measured value is dominated by systematic effects. See the text for details.

T (K)	P_{Rb} (Expt.)	P_{Rb} (A)	P_{Rb} (B)	P_{Rb} (C)
451	0.579±0.042	0.8265	0.7853	0.7500
443	0.665±0.049	0.8853	0.8549	0.8327
458	0.474±0.035	0.7182	0.6670	0.6212

To examine this discrepancy, the calculations were modified in several ways. Since the expansion optics were changed slightly from the design configuration to account for the longer cell, a direct measurement of the laser power density (0.27 W cm^{-2}) was made at the cell location and used as input to all our theoretical calculations. A correction for an unpolarized layer of Rb near the cell wall was also included. The thickness of this layer has been estimated to be about 40 μm [11], making its contribution to the average Rb polarization in the cell negligible. We have included this layer because of the attenuation to the incoming laser beam power.

All of the previous calculations assumed that the Rb vapor was uniform in thickness. However, the cell used had a cylindrical cross section and the thickness varies as illustrated in Fig. 7. The calculations were then modified to average the expected Rb polarization along each chord of the cylinder and then all chords were averaged to determine the cell average. These cell average results are shown in Table II as the $P_{\rm Rb}$ (A) predictions. These theoretical predictions are still much larger than the measured polarizations.

In the previous calculations, it has been assumed that the incident laser light is 100% circularly polarized. For the measurements presented in this paper, this was not the case. Unfortunately, in the limited space available in our apparatus, it was not possible to install a "clean up" polarizer before the quarter wave plate. This led to incomplete circular polarization of the incident laser beam. The amount of polarization was measured using a liquid crystal circular polarizer. This device transmits left-handed polarized light with better than 97% efficiency, while it reflects right-handed polarized light (transmission $< 0.03\%$). Measurements with this device indicated that $5(\pm 2)\%$ of the incident laser photons had the wrong helicity. The linearity of the diode laser polarization was also measured and gave a ratio of 20:1, consistent with the above measurement.

To accurately account for the impact of wrong helicity photons, we rewrote the optical pumping rate equation assuming the presence of both helicities, so that

$$\frac{d\rho_-}{dt} = -\gamma^+\rho_- + \gamma^-\rho_+ + \frac{\Gamma_{\rm SD}}{2}(\rho_+ - \rho_-), \qquad (15)$$

where $\rho_\pm$ is the probability of finding a Rb atom in the $m_s = \pm 1/2$ magnetic substate. To be consistent with the formulas in Sec. II, γ^+ is the absorption rate for correct helicity photons and γ^- is the absorption rate for wrong helicity photons. This is a different treatment of incomplete circular polarization than in previous work [11], which we believe to be more illuminating because photons propagating parallel to a magnetic field cannot induce π $(\Delta m_s = 0)$ electric dipole transitions. When this rate equation is solved, we obtain the analogous equations [to Eqs. (1) and (2)] for the Rb polarization, where

$$P_{\rm Rb}(z) = \frac{\gamma^+(z) - \gamma^-(z)}{\gamma^+(z) + \gamma^-(z) + \Gamma_{\rm SD}} \qquad (16)$$

and the power absorbed is

$$\Delta I^\pm = -\Delta z[{\rm Rb}]\gamma^\pm(z)\frac{\Gamma_{\rm SD} + 2\gamma^\mp(z)}{\gamma^+(z) + \gamma^-(z) + \Gamma_{\rm SD}}. \qquad (17)$$

Therefore, when the laser beam enters the Rb vapor environment, the correct helicity and wrong helicity photon beams propagate independently. The impact of incomplete circular polarization is shown in Fig. 8. The calculations shown in Fig. 3 for 7 amagat of ^{3}He buffer gas have been modified to include wrong helicity photons in the incident diode laser beam. Figure 8 shows the effect as the amount of wrong helicity photons is varied between 0% and 15%.

We then added the effect of incomplete polarization to our theoretical prediction of the average Rb polarization. These results are shown in Table II as the $P_{\rm Rb}$ (B) predictions. For these predictions, 5% of the incoming beam was assumed to be wrong helicity photons. Again the results are larger than the measured values.

To further explore this discrepancy, we did a detailed calculation of the transmission of the laser light through the cell wall. In particular, in light of the above results on incomplete polarization, we were very interested in any changes to the polarization of the incoming laser light. As shown in Fig. 7, the laser light is not normally incident on the glass cell but instead is incident at angles up to 90° away from the normal. A solution of the Fresnel equations for this situation, assuming that the incident

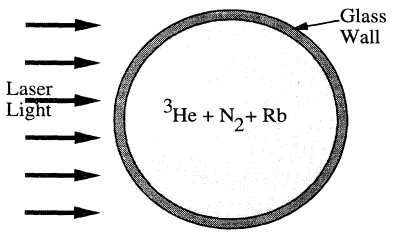

FIG. 7. Cross section of a typical ^{3}He target cell showing incident laser (pumping) light.

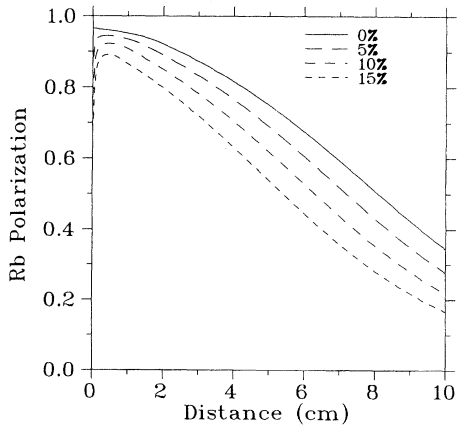

FIG. 8. Effect of incomplete circular polarization on the the induced Rb polarization in 7 amagat of ^{3}He buffer gas. Curves are shown for values of the opposite helicity fraction of the incoming beam between 0% and 15%.

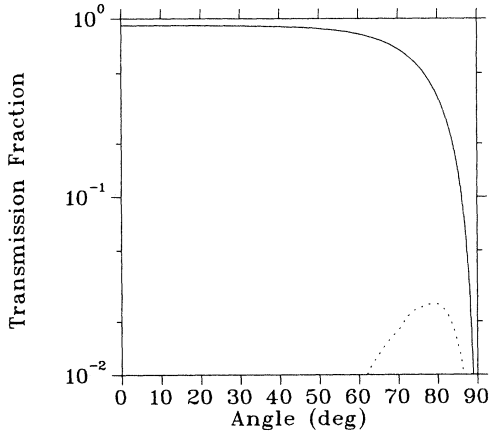

FIG. 9. Solutions to the Fresnel equations for 100% circularly polarized light shown as a function of incident angle on the cell wall (0°=normal incidence). The solid line shows the fraction of incident light transmitted in the same circular polarization state as the incident beam. The dotted curve shows the fraction that is transmitted in the "wrong" circular polarization state.

light was 100% left-handed circularly polarized, leads to the results shown in Fig. 9. The fractions of the incident laser light transmitted as left-handed (solid curve) and right-handed (dotted curve) circularly polarized light are shown as a function of angle of incidence (away from the normal). Near normal incidence, the transmitted light is 92% of the total incident light and has the same helicity. This 8% difference comes from the 4% reflection per surface. At large angles, the total amount of transmitted light decreases and a small amount of opposite helicity light is transmitted. These calculations were done assuming that the radius of the cell was much larger than the thickness of the glass and thus the light within the cell was parallel to the incident light.

The results for transmission through the cell wall have been added to the cell average calculations, which assume a 5% wrong helicity photon content of the incident beam. These results for Rb polarization in the cell are included in Table II as the P_{Rb} (C) results and are 25–30% larger than the measured average Rb polarizations.

V. CONCLUSIONS

The discrepancy between the calculated theoretical Rb polarization and the measured average Rb polarization as measured by the ^{3}He polarization has been seen in previous work. The effect has been less pronounced in cells with smaller total volume than the cells used in the present study. In similar sized cells to those used here, the ^{3}He polarization has been limited to about 60%, while the available laser power should have pumped the cell to about 80% [11]. The investigation of the effects of incomplete polarization and transmission of the laser light through the cell walls presented here has only been able to account for part of this difference. As cited in previous work [11], the remainder of this difference may result from shadowing of the cell (by its supports) and nonuniform power density in the expanded beam. Variations in the power density of as much as 40% in the expanded laser beam have been measured. In the future, it would be interesting to make measurements of average Rb polarization using a very uniform laser beam.

A very obvious explanation for the lower Rb polarization would be an increased value of Γ_{SD} over the value used in our calculations. In a recent publication [25], Wagshul and Chupp have examined the spin destruction of polarized Rb vapor in great detail. In particular, they measured the effect of the Rb nuclear spin on the electronic spin destruction by chopping the pumping laser beam. Their work shows that the Rb nuclear spin slows down the time scales required to polarize and destroy the polarization of the Rb atom by the same amount. Therefore, the steady state Rb polarization given by Eq. (1) (which ignores the Rb nuclear spin) should be appropriate. Furthermore, the value of Γ_{SD} used in our calculations was deduced from the measurements by Larson *et al.* [11] of the transmission of circularly polarized light through cells very similar to the one used in this work. In these measurements, the same model was used as in this work. In this model, which is summarized by Eqs. (1) and (2), all sources of Rb spin destruction (except the cell walls) are described by a single spin-destruction rate Γ_{SD}. The value of Γ_{SD} is determined by the steady state attenuation of the pumping laser beam. Thus, in a self-consistent way, the appropriate value of Γ_{SD} has been used in this work.

Our observation that the maximum ^{3}He polarization decreases with increasing cell size indicates that radiation trapping may be limiting the Rb polarization. It is well known that alkali-metal vapor polarizations can be severely limited by radiation trapping in a weak magnetic field [26]. This effect should be mitigated by the quenching by the N_2 buffer gas in the cell. We have calculated the quenching efficiency for one of our cells to be $> 95\%$. However, the small quenching inefficiency may lead to lower Rb polarization. We are planning measurements of Rb polarization as a function of incident laser power to study radiation trapping effects. If radiation trapping is limiting the Rb polarization in these targets, additional quenching gas may improve their performance.

The Rb polarization may be smaller than calculated due to lower optical pumping efficiency in the wings of the collisionally broadened $D1$ resonance. In Eq. (3), the optical pumping efficiency was assumed to be independent of frequency near the $D1$ resonance. The optical pumping efficiency is the probability that the absorbed circularly polarized photon is absorbed by the desired magnetic substate and decays into the opposite magnetic substate. In the absence of collisional broadening, the optical pumping efficiency at the $D1$ resonance is 1/2. However, in the presence of a buffer gas, off-resonant photons can be absorbed by Rb atoms that are close enough to buffer gas atoms to form excimer molecules. This leads to the collisionally broadened $D1$ absorption line shown in Fig. 1. Near the central frequency of the absorption line shown in Fig. 1, the optical pumping efficiency is

1/2. However, in the wings of the resonance, the optical pumping efficiency may be smaller. In the limit of very small average internuclear spacing, the Coulomb interactions of the excited Rb electron with the He atom become larger than the spin-orbit interactions in the core of the Rb atom and the molecular coupling scheme becomes Hund's case a. In this high-density limit, some of the circularly polarized photons may be absorbed by the wrong magnetic substate [28]. For the moderate collisional broadening in this work, the effect should not be very pronounced, but may still lead to measurable effects. This effect is closely related to measurements of the magnetic circular dichroism of alkali-metal vapors in high-pressure noble gases [29]. Measurements of the Rb polarization as a function of laser frequency using a narrow band (Ti:sapphire) laser would be useful to quantify the size of this effect. In their recent paper, Wagshul and Chupp [25] report measurements of this type for N_2 buffer gas densities of 0.5, 1.5, and 4.1 amagat. The results for the two smaller densities show reduced pumping efficiencies in the wings of the resonance. However, for the highest density measurements, the effect was not seen. Similar measurements for noble buffer gasses are still needed to estimate the size of this effect for the present results.

Another explanation for the difference between these theoretical calculations and the measured average Rb polarizations may be the effect of the laser light reflected back into the cell from the far wall (as seen by the laser). Much of this reflected light has the wrong polarization, which we have seen leads to significantly lower Rb polarizations and the need for greater laser power. We have estimated the fraction of incident laser light reflected back into the cell for the conditions of these measurements and found it to be between 5% and 7%. The impact of this reflected light has not been more completely examined because it significantly changes the nature of the theoretical calculations, which for this work have been one dimensional. We plan to present the complete calculations in a future paper.

The value of γ_{SE} measured in this work agrees with the results of Ref. [11], but is a factor of 2 lower than the results of Refs. [2] and [13]. Ultimately, additional measurements will be required to resolve this situation. Significantly, a new measurement has been made using a different method, which adds additional data to this discussion. A recent estimate of $\langle \sigma_{SE} v \rangle$ [27] has been made using the shift in the Rb electron paramagnetic resonance line. While this result is model dependent, their estimate is consistent with the measurements of $\langle \sigma_{SE} v \rangle$ [2,13], which are a factor of 2 larger than the value one would extract from this work. One explanation for this discrepancy would be that the Killian formula [Eq. (14)] is not correct at 450 K and [Rb] is actually a factor of 2 lower. However, if [Rb] is smaller, the theoretical values for the average Rb polarizations would be larger, making the disagreement between calculation and measurement worse.

From the outset, the goal of this work was to establish whether these new high-power diode laser arrays would make a suitable light source for polarized ^{3}He targets. The highest polarization of ^{3}He achieved in our studies was 53%, which is comparable to the 55–60 % polarization achieved in this same target cell when pumped with Ti:sapphire lasers [24]. This comparison is even more favorable when considering the fact that the diode laser used in these studies was not optimally expanded, had lower output power due to small aperatures in the optics, and was incompletely polarized. Therefore, the conclusion is that diode laser arrays are effective light sources for spin-exchange polarized ^{3}He targets.

ACKNOWLEDGMENTS

The authors gratefully acknowledge D. Dehnhard for supplying the diode laser used in these studies. We also acknowledge the support of the LAMPF staff and particularly, P. Reed, M. Murray, and L. Duncan in constructing the power supply for the diode laser. The authors thank W. Happer, N. Newbury, G. Cates, and P. Levy for very useful discussions. Our thanks also go out to all those who participated in LAMPF experiment 1267. This work was supported by NSERC (Canada) and DOE grants.

[1] P. Anthony *et al.*, Phys. Rev. Lett. **71**, 959 (1993).
[2] K.P. Coulter, A.B. McDonald, W. Happer, T. Chupp, and M. Wagshul, Nucl. Instrum. Methods A **270**, 90 (1988).
[3] K.P. Coulter, A.B. McDonald, W. Happer, T. Chupp, and M. Wagshul, Nucl. Instrum. Methods A **288**, 463 (1990).
[4] F. Tasset, T.E. Chupp, J.P. Pique, A. Steinhof, A. Thompson, E. Wasserman, and M. Ziade, Physica B **180&181**, 896 (1992).
[5] A. Rahav *et al.*, Phys. Rev. C **46**, 1167 (1992).
[6] E.J. Brash *et al.* (unpublished).
[7] N.R. Newbury, A.S. Barton, P. Bogorad, G.D. Cates, M. Gatzke, B. Saam, L. Ham, R. Holmes, P.A. Souder, J. Xu, and D. Benton, Phys. Rev. Lett. **67**, 3219 (1991); **69**, 391 (1992).
[8] A.S. Barton, P. Bogorad, G.D. Cates, H. Mabuchi, H. Middleton, N.R. Newbury, R. Holmes, J. McCracken, P.A. Souder, J. Xu, and D. Tupa, Phys. Rev. Lett. **70**, 758 (1993)
[9] B. Larson *et al.*, Phys. Rev. Lett. **67**, 3356 (1991).
[10] M. Espy *et al.* (unpublished).
[11] B. Larson, O. Hausser, P.P.J. Delheij, D.M. Whittal, and D. Thiessen, Phys. Rev. A **44**, 3108 (1991).
[12] T.E. Chupp and M. Wagshul, Phys. Rev. A **40**, 4447 (1989).
[13] T.E. Chupp, M. Wagshul, K.P. Coulter, A.B. McDonald, and W. Happer, Phys. Rev. C **36**, 2244 (1987).
[14] T.E. Chupp, R.A. Loveman, A.K. Thompson, A.M. Bernstein, and D.R. Tieger, Phys. Rev. C **45**, 915 (1992).
[15] W. Happer, Rev. Mod. Phys. **44**, 169 (1972).
[16] R.J. Knize, Phys. Rev. A **40**, 6219 (1989).

[17] F.A. Franz and C. Volk, Phys. Rev. A **14**, 1711 (1976).
[18] W. Lorenzon, T.R. Gentile, H. Gao, and R.D. McKeown, Phys. Rev. A **47**, 468 (1993).
[19] N.R. Newbury, A.S. Barton, G.D. Cates, W. Happer, and H. Middleton, Phys. Rev. A **48**, 4411 (1993).
[20] O. Hausser, B. Larson, E.J. Brash, W.J. Cummings, W. Lorenzon, and P.P.J. Delheij, in *Polarized Ion Sources and Polarized Gas Targets*, edited by L.W. Anderson and Willy Haeberli, AIP Conf. Proc. No. 293 (AIP, New York, 1993), pp. 253–256.
[21] R.M. Herman, Phys. Rev. **137**, A1062 (1965).
[22] T. Killian, Phys. Rev. **27**, 578 (1926).
[23] A. Steinhof, Physica B **180&181**, 955 (1992).
[24] B. Larson *et al.*, Phys. Rev. C **49**, 2045 (1994).
[25] M.A. Wagshul and T.E. Chupp, Phys. Rev. A **49**, 3854 (1994).
[26] D. Tupa and L.W. Anderson, Phys. Rev. A **36**, 2142 (1987).
[27] N.R. Newbury, A.S. Barton, P. Bogorad, G.D. Cates, M. Gatzke, H. Mabuchi, and B. Saam, Phys. Rev. A **48**, 558 (1993).
[28] W. Happer (private communication).
[29] M.A. Salam, A. Kponou, B. Suleman, and W. Happer, Phys. Rev. Lett. **47**, 643 (1981).